Civil Engineering Dimension
https://ced.petra.ac.id

Probabilistic Analysis of the Failure Time of Concrete-Filled Steel Tube (CFST) Columns under Post-Blast Fire Loading

Afaghi-Darabi, A.[1], Moradi, M.[2]*, and Rezaei, S.[3]
[1] Ph.D. Candidate of Earthquake Engineering, Babol university of Technology, Babol, IRAN
[2,3] Assistant Professor, University of Science and Technology of Mazandaran, Behshahr, IRAN

DOI: https://doi.org/10.9744/ced.28.2.230-248

Article Info:
Submitted: Aug 28, 2025
Reviewed: Oct 12, 2025
Accepted: May 04, 2026

Keywords:

post-blast fire,
CFST columns,
probabilistic analysis,
sensitivity analysis,
random variables.

Corresponding Author:

Moradi, M.
Assistant Professor, University of Science and Technology of Mazandaran, Behshahr, IRAN
Email: m.moradi@mazust.ac.ir

Abstract

This study examines the behavior and resistance of concrete-filled steel tube (CFST) columns under post-blast fire conditions, where prior explosions cause initial structural damage affecting fire performance. A blast equivalent to 20 kg TNT at a 1.5 m distance was simulated, followed by fire exposure. Seven numerical models were developed in ABAQUS, considering variations in column type, dimensions, length, and boundary conditions. A sensitivity analysis using the tornado diagram method evaluated the impact of random variables. Results show that CFST columns have significantly greater resistance than hollow steel columns in such scenarios. Among the variables, steel yield strength, concrete compressive strength, and axial load had the most influence on failure time. Probabilistic analysis further indicated that columns with larger diameters, even with increased height to maintain constant slenderness ratio, performed better, achieving an average failure time of 10829 seconds compared to other specimens under similar conditions.

INTRODUCTION

Concrete-filled steel tube (CFST) columns consist of hollow cylinders with rectangular, circular, or diamond-shaped cross-sections, which are filled with concrete [1]. Due to their advantages, these columns are widely employed in high-rise structures and in seismically active regions [2]. The steel tube acts as a confinement for the concrete, thereby enhancing both the load-bearing capacity and ductility of the concrete [3]. The presence of concrete within the steel tube also delays both global and local buckling of the steel, consequently increasing the load-bearing capacity of the steel [4]. Moreover, despite the relatively low stiffness and fire resistance of steel, the concrete infill provides CFST columns with substantial fire resistance and improved overall stiffness [5,6].

Extensive research has been conducted on the behavior of CFST columns at elevated temperatures. These studies have demonstrated that the fire resistance of CFST columns increases with larger cross-sectional dimensions and higher concrete strength [7–9]. When a CFST column is subjected to blast loading, the explosion reduces its load-bearing capacity and induces residual deformations [10,11]. Assessing the damage of CFST columns under blast loading is closely related to the safety of many structures [12]. Studying steel tube columns with various cross-sectional shapes under near-field blast loading is of particular importance [11].

Engineering structures are constantly exposed to various hazards [13,14]. Such events cause greater structural damage when they occur sequentially [15–17]. Given the frequent occurrence of explosions and terrorist attacks

Note : Discussion is expected before November, 1st 2026, and will be published in the "Civil Engineering Dimension", volume 29, number 1, March 2027.
ISSN : 1410-9530 print / 1979-570X online
Published by : **Petra Christian University**

worldwide, the likelihood of damage to conventional building structures due to blasts is increasing. Therefore, the dynamic characteristics and blast resistance performance of CFST columns require more attention than ever. Furthermore, explosions are often accompanied by fires, making it necessary to evaluate the combined effect of sequential blast and post-blast fire loading on different structural elements. To date, few studies have specifically examined the effect of Post-Blast Fire on CFST columns. In this study, an effort has been made to examine the behavior of CFST columns subjected to a blast followed by fire loading, in order to assess their response under post-blast fire conditions.

Craveiro et al. and Cai et al. [18,19] experimentally examined the fire performance and residual strength of CFST and engineered cementitious composite-encased columns, emphasizing the effects of material composition and confinement on thermal resistance. Tkalenko et al. and Boursas et al. [20,21] presented analytical and numerical investigations that highlighted the influence of slenderness ratio, applied load level, and composite interaction on the structural response of CFST columns under fire conditions. More recently, a numerical study by Buildings proposed an advanced finite element model to simulate the thermo-mechanical behaviour of CFST columns at elevated temperatures, showing good agreement with full-scale experimental results [22]. These recent studies indicate substantial progress in the understanding of CFST columns subjected to fire loading; however, research addressing combined hazard scenarios, especially the sequential effects of blast and fire, remains scarce. Therefore, the present study aims to contribute to this research gap by developing and validating a coupled ABAQUS model to investigate the deterministic and probabilistic behaviour of CFST columns under post-blast fire conditions.

Research Significance and Novelty of the Study

Concrete-Filled Steel Tube (CFST) columns have been widely studied due to their superior load-bearing capacity, stiffness, and ductility under extreme conditions. Earlier research has extensively examined their fire performance, revealing that temperature, cross-sectional geometry, and material strength strongly influence resistance and failure modes [2,24,25]. Similarly, several investigations have focused on the blast response of CFST columns, demonstrating that the steel tube confinement enhances impact resistance and energy absorption capacity [11,23].

However, nearly all of these studies have considered fire and blast as isolated phenomena, whereas in real scenarios, these hazards frequently occur sequentially - a blast followed by a fire. Such consecutive loading can induce local buckling, residual deformations, and material degradation that significantly modify the thermal and structural response during fire exposure. Despite the practical importance of this phenomenon, the literature review shows that studies explicitly addressing the post-blast fire behavior of CFST columns are extremely limited [12,18,20]. Moreover, the effects of uncertainty in material and geometric properties under these combined hazards have not been examined in a probabilistic framework.

To bridge this research gap, the present study proposes a validated, probabilistic, and sensitivity-based modeling framework for evaluating the post-blast fire resistance of CFST columns. The major contributions can be summarized as follows:

1. Sequential Multi-Hazard Simulation:
   A coupled finite element model is developed in ABAQUS to simulate the combined effects of blast and subsequent fire. Unlike prior studies analyzing each hazard separately, this integrated approach captures the interactive deterioration mechanisms that govern structural resistance under realistic extreme events.
2. Probabilistic Reliability Assessment:
   Building on the deterministic methods used in previous fire and blast studies, this research incorporates a Monte Carlo simulation framework to evaluate the statistical distribution of failure time, enabling a reliability-based interpretation of CFST performance under compound hazards [14].
3. Sensitivity-Based Parameter Analysis:
   A Tornado Diagram Analysis (TDA) approach is applied to quantify the relative influence of uncertain parameters, including steel yield strength, concrete compressive strength, and axial load, on failure time. This represents a novel application of sensitivity methods for CFST columns under combined blast–fire conditions [13].
4. Validated Dual-Phase Modeling:
   Both the blast and fire sub-models are validated independently using benchmark experimental data [23,25] prior to integration, ensuring accuracy and physical consistency of the simulation framework.
5. Scientific and Practical Contribution:
   The results reveal that prior blast exposure can reduce the fire resistance of CFST columns by up to 13%, while concrete infill significantly mitigates this reduction by enhancing confinement and delaying global buckling.

These findings offer a scientific foundation for performance-based design and multi-hazard resilience assessment of CFST columns.

In summary, this study advances current knowledge by presenting a comprehensive multi-hazard, probabilistic, and sensitivity-driven methodology for assessing CFST column behavior under post-blast fire conditions. The proposed framework not only fills a major gap identified in the literature but also provides new insights for reliability-based design of critical infrastructure subjected to consecutive extreme events.

NUMERICAL MODEL DESCRIPTION

To investigate the behavior of CFST columns under post-blast fire loading, a finite element model was developed in ABAQUS. This model captures the effects of the blast and temperature variations at different points of the CFST column during fire loading, and evaluates their impact on the mechanical behavior of the column. The explosive charge was modeled as 20 kg of TNT, positioned 1.5 meters from the column's central axis at mid-height. To apply the blast loading, the ConWep model in ABAQUS was employed. Due to its high accuracy and reasonable computational cost compared to other methods, this model is widely used in blast research. In this study, the explosion type was defined as an air blast. The relationship used in the model is derived from multiple experimental blast tests and is provided by default in ABAQUS; only simple input parameters such as the explosive weight and its location relative to the column are required.

For fire loading, a heat transfer analysis was first conducted in ABAQUS to measure temperature variations at different points within the specimen. These thermal data were then input into a global static analysis to evaluate the mechanical response of the column under elevated temperatures. In this model, the column has a height of 3200 mm and is assumed to be fixed at one end and pinned at the other.

Considering that combined blast and fire behavior has not yet been experimentally modeled in laboratories, and that prior studies have not conducted numerical modeling of the simultaneous effects of fire and blast, two separate models were developed in this study: one subjected to blast loading and the other to fire loading. Each model was validated independently using experimental data and prior research. Subsequently, both models were implemented in ABAQUS, with blast and fire loading applied sequentially, and the mechanical response of the column was assessed. Table 1 presents the specifications of the specimens considered in this study.

Table 1. Specifications of the Specimens Considered in this Study

Sample	Dimension	Height	Thickness	Fy	Fc	Support	Axial Load	DCR
C1	240	3200	4	358	48	Fixed-Pinned	820	0.45
C2	240	3200	4	358	0	Fixed- Pinned	386	0.45
C3	200	3200	4	358	48	Fixed- Pinned	615	0.45
C4	300	3200	6	358	48	Fixed- Pinned	1400	0.45
C5	200	2700	4	358	48	Fixed- Pinned	820	0.45
C6	300	4000	6	358	48	Fixed- Pinned	820	0.45
C7	240	3200	4	358	48	Fixed-Fixed	820	0.45

Fire Phase Modeling and Validation

To validate the finite element (FE) model developed in ABAQUS, the experimental results reported by Lie and Chabot [25] from the National Research Council of Canada (NRCC) were used. The original tests were carried out in a large-scale furnace with internal dimensions of 2642 × 2642 mm and a height of 3048 mm, which was internally lined with ceramic insulation panels. A schematic of the furnace and the column setup is shown in Figure 1.

Each CFST specimen was subjected to a constant axial load applied by hydraulic jacks with a total capacity of 9778 kN, in order to simulate the gravity load from upper stories of a building. The applied load was maintained constant throughout the heating process. The axial shortening of the specimen was continuously measured using displacement sensors with an accuracy of 0.002 mm, and the temperature distribution was monitored by thermocouples installed along the height and thickness of the column.

The specimen selected for validation in this study had a total height of 3810 mm, outer diameter of 219.1 mm, and steel wall thickness of 8.18 mm. Both ends of the column were restrained (fixed–fixed). Two vent holes were drilled at 457 mm from each end to release the compressed air inside the steel tube during heating. The compressive strength of concrete was 31.7 MPa, and the yield strength of steel was 350 MPa. The applied axial load was 525 kN.

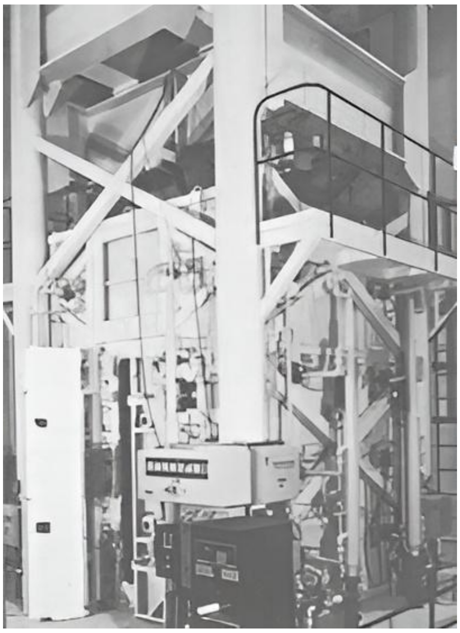

Figure 1. Column Test Furnace [25]

Prior to heating, the axial load was applied and maintained for 45 minutes to ensure that the specimen remained stable under sustained compression before fire exposure. The fire temperature followed the ASTM E119 standard fire curve, applied uniformly along the central portion of the column.

$$T = 20+750[1\text{-}exp(\text{-}3.79533t)]+170.41t \tag{1}$$

where t represents time in hours and T denotes temperature in degrees Celsius. A finite element model was developed in ABAQUS, as illustrated in Figure 2, and validated using the experimental results. Initially, a heat transfer analysis was conducted to determine the temperature distribution along the column height and across its cross-section, followed by a global static analysis to assess the mechanical behavior of the column.

In this model, the column had a total height of 3810 mm, of which only the middle portion, 3084 mm in height, was exposed to fire. The upper and lower portions were considered as ceiling regions and were not directly subjected to fire. The temperature distribution along the height of the column was assumed to be uniform, whereas a temperature gradient was present across the cross-section [25].

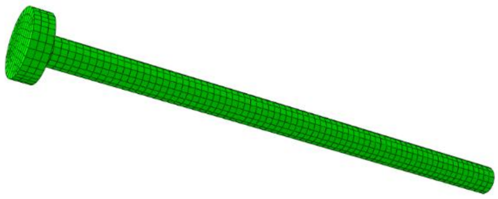

Figure 2. Finite Element Model of the Column Specimen Developed in ABAQUS

In this model, the density of steel at different temperatures was considered constant at 7850 kg/m^3 in accordance with Eurocode 3. For concrete, the density is temperature-dependent and is calculated according to the relations provided in Eurocode 2 [26,27]. The specific heat of steel was obtained using Eurocode 3, while that of concrete was obtained from Eurocode 4 [26,28]. The coefficient of thermal expansion for concrete was taken as 6×10^{-6} according to the research by Hong and Varma [29], and for steel, it was defined using the relation proposed by Lie and Irwin [30]. Thermal conductivity for both steel and concrete was adopted from Eurocode 4 [28].

The mechanical properties of steel and concrete, including the stress-strain curve and elastic modulus at elevated temperatures, were incorporated. To account for the plastic behavior of concrete, the Concrete Damaged Plasticity (CDP) model was used, which was developed by Lee and Fenves [31] and implemented in ABAQUS. Concrete tensile strength was calculated using the relations provided by Eurocode 1-1-1992 at ambient temperature, and Eurocode 2-1-1992 for elevated temperatures [32]. The elastic modulus of concrete was calculated using the Anderberg and Thelandersson relation [33].

The Coulomb friction coefficient between the steel and concrete contact surfaces was taken as 0.25, according to Ellobody, Young and Lam [34]. Separation between the two surfaces under tension was allowed, while no penetration was permitted under compression. A rigid connection was defined in the direction normal to the surfaces. The thermal resistance between steel and concrete was modeled according to the relation proposed by Ghojel [35]. To consider the dominant buckling mode of the CFST column in ABAQUS, a preliminary buckling analysis was performed to determine the deformation patterns under failure modes. Subsequently, a heat transfer analysis was conducted to evaluate the temperature distribution at various points of the column under fire loading. Finally, a global static analysis was performed to assess the mechanical response of the CFST column at different temperatures.

The column was modeled with three components: the steel tube, the top cap, and the concrete core, all represented using solid elements. For the heat transfer analysis, the same geometry and meshing as in the buckling analysis were used. Heat was applied to the column through convection, radiation, and conduction. For convection, a coefficient of 25 W/m²·°C was applied to surfaces exposed to fire, and 9 W/m²·°C for the top and bottom surfaces not directly exposed. In radiation, the emissivity of the steel surface was taken as 0.5. For conduction, thermal conductivity values for steel and concrete were used. Heat transfer elements of type DC3D8 from the heat transfer element family were employed.

To validate the model, the results of the heat transfer and global static analyses were compared with experimental data. It was assumed that the fire initially covered the entire column height, resulting in a uniform temperature distribution along the height. Figure 3 presents the heat transfer results at five points.

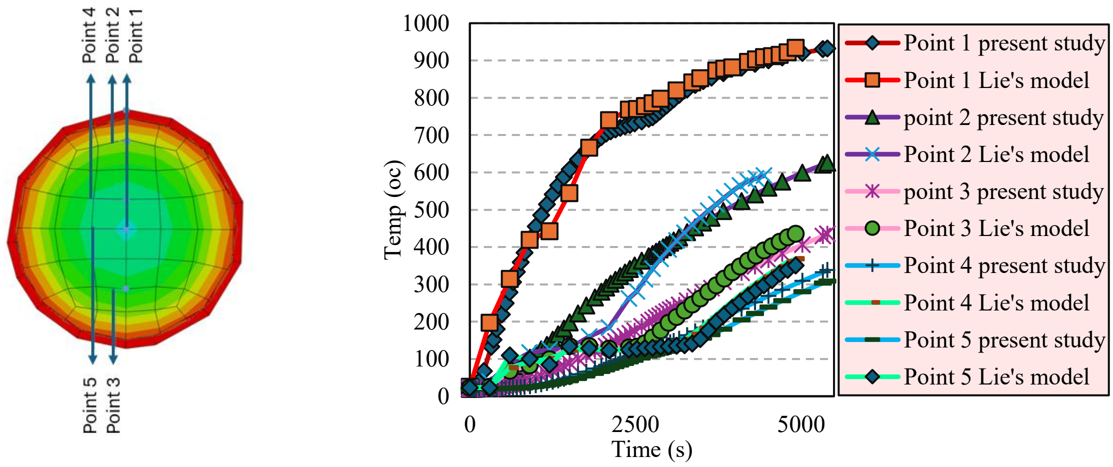

a) b)

Figure 3. Validation Results of the Fire Phase: (a) Temperature Variations at Different Points across the Column Cross-section, (b) Comparison between Experimental and Numerical Results obtained in the Present Study

Figure 3(b) illustrates the temperature history at five specific points on the column cross-section shown in Figure 3(a), which can be compared with the readings obtained from thermocouples embedded in the experimental specimen. As observed, during the initial stage of temperature rise, the experimental specimen experiences a rapid increase in temperature, followed by a period of temperature stabilization, and then a subsequent rise. In contrast, in the simulated specimen, the temperature increases gradually until it reaches its maximum value. The comparison of these curves indicates that the heat transfer simulation of the CFST column demonstrates acceptable accuracy.

In Figure 4, the axial deformation results of the upper portion of the column obtained from the global static analysis are compared with the experimental measurements. As shown in Figure 4, a good agreement is observed between the experimental and numerical results.

In order to ensure the accuracy and convergence of the finite element model, a mesh sensitivity analysis was performed. The sensitivity analysis was based on the fire resistance duration of the CFST column. Three mesh configurations, labeled A, B, and C, were evaluated with different element sizes for the steel tube and concrete core, as summarized in Table 2. The results showed that refining the mesh beyond Type B (concrete mesh size = 35 mm, steel mesh size = 50 mm) caused no significant change in the predicted fire resistance time or deformation response. Therefore, Type B was selected for the final analysis as it ensured convergence and provided an optimal balance between accuracy and computational efficiency.

Table 2. Mesh Configurations used in the Sensitivity Analysis

Type	Steel mesh size (mm)	Concrete mesh size (mm)	Fire resistance time (s)
A	50	40	4864
B	50	35	4963
C	40	35	4987

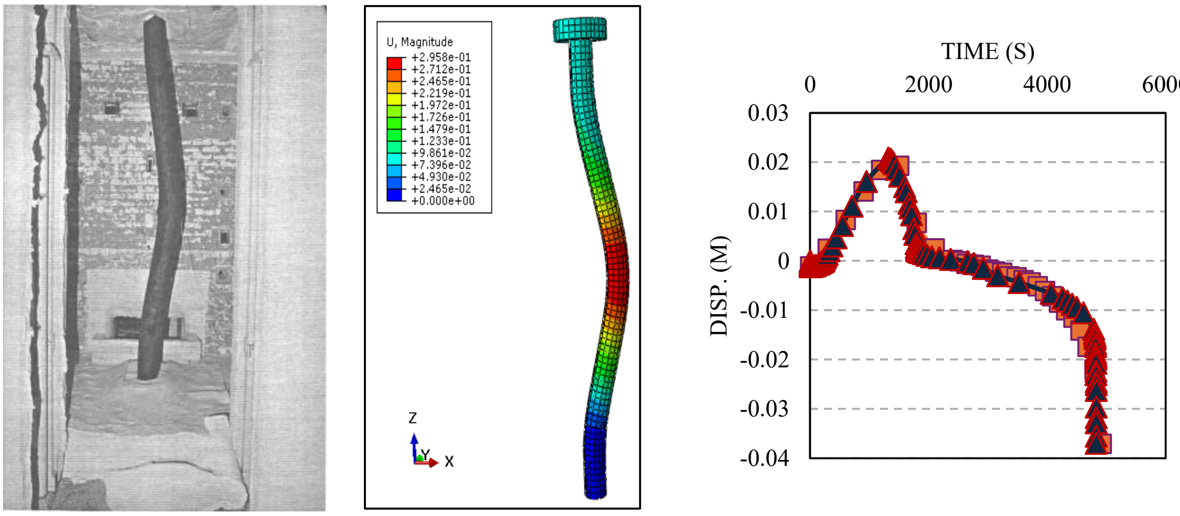

a) b) c)

Figure 4. Validation Results of Axial Deformation during the Fire Phase: (a) Experimental Model, (b) Numerical Model, (c) Comparison of Numerical Values between the Experimental and Numerical Specimens

Modeling and Validation of the Specimen under Blast Loading

To validate the numerical model, an experimental specimen tested at PLA University of Science and Technology, China, in 2014 was utilized. The specimen had a diameter of 200 mm, a thickness of 2.8 mm, and a height of 2500 mm. In the experiment, axial loads were applied to the specimens using hydraulic jacks. The column ends were designed with pinned–pinned boundary conditions. The TNT charge used in this test had a weight of 35 kg and was positioned at a distance of 1500 mm from the mid-height of the column [23].

Since the mechanical properties of steel and concrete vary significantly under high strain-rate loading, a constitutive model that incorporates strain-rate effects was required. In this study, the Dynamic Explicit solver in ABAQUS was employed to analyze the column behavior under blast loading. For concrete properties, the constitutive model proposed by Song [36] was adopted. Considering that the confinement effect of the steel tube enhances both compressive strength and ductility of the core concrete, and that strength enhancement is already accounted for in ABAQUS, the ductility effect was introduced using the parameter ζ in Song's model [36].

$$\frac{\sigma_c}{\sigma_0} = \begin{cases} 2\frac{\varepsilon_c}{\varepsilon_0} - (\frac{\varepsilon_c}{\varepsilon_0})^2 & \frac{\varepsilon_c}{\varepsilon_0} \leq 1 \\ \beta(\frac{\varepsilon_c}{\varepsilon_0} - 1)^\eta + \frac{\varepsilon_c}{\varepsilon_0} & \frac{\varepsilon_c}{\varepsilon_0} > 1 \end{cases} \tag{2}$$

where $\varepsilon c/\varepsilon 0$ denotes the ratio of concrete strain to the reference strain at 20 °C, and σ_c/σ_0 represents the ratio of concrete stress to the reference stress at 20 °C. The value of $\varepsilon 0$ can be calculated using Equation (3).

$$\varepsilon_0 = (1300 + 12.5f_c + 800\zeta^{0.2}) \times 10^{-6} \tag{3}$$

$$\zeta = \frac{A_s f_y}{A_c f_{ck}}$$

where ζ is the confinement effect coefficient, as the cross-sectional area of steel, fy the yield strength of steel, Ac the cross-sectional area of concrete, and fck the characteristic compressive strength of concrete. The values of β and η can be calculated from Equations (4) and (5), respectively.

$$\beta = \begin{cases} (2.36 \times 10^{-5})^{[0.25+(\zeta-5)^7]}(f_c)^{0.5} \times 0.5 \geq 0.12 & Circular\ Column \\ \dfrac{{f_c}^{0.1}}{1.2\sqrt{1+\zeta}} & Rectangular\ Column \end{cases} \tag{4}$$

$$\eta = \begin{cases} 2 & Circular\ Column \\ 1.6 + 1.5 / \dfrac{\varepsilon_c}{\varepsilon_0} & Rectangular\ Column \end{cases} \tag{5}$$

Furthermore, to account for the strain-rate effect in this relation, Equation (6) is applied.

$$\frac{f_c}{f_{cs}} = (\frac{\varepsilon^{\cdot}}{\varepsilon^{\cdot}{}_s})^{1.026\alpha_s} \qquad \varepsilon^{\cdot}{}_s \leq 30s^{-1} \tag{6}$$

$$= \gamma_s(\frac{\varepsilon^{\cdot}}{\varepsilon^{\cdot}{}_s})^{1/3} \qquad \varepsilon^{\cdot}{}_s > 30s^{-1}$$

In the above relations, fc denotes the dynamic compressive strength at a strain rate of $\varepsilon^{\cdot}$, while fc represents the static compressive strength. The strain rate $\varepsilon^{\cdot}$ ranges between 3×10^{-6} and $300\ s^{-1}$. The static strain rate $\varepsilon^{\cdot}s$ is taken as 3×10^{-6}. The parameters αs and γs can be calculated using Equations (7) and (8), respectively.

$$\propto = 1/(5 + \frac{9f_{cs}}{f_{c0}}) \tag{7}$$

$$\log \gamma_s = 6.156 \propto -2 \tag{8}$$

The mechanical properties of steel are defined using a bilinear stress–strain curve, as illustrated in Figure 5.

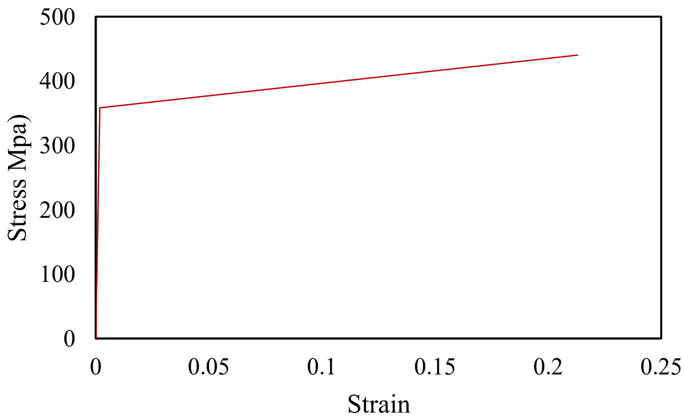

Figure 5. Stress–Strain Curve of Steel [30]

To incorporate the effects of dynamic loading conditions on steel, the yield stress of steel must be multiplied by the Dynamic Increase Factor (DIF). In this study, the Cowper and Symonds model is adopted, as expressed in Equation (9) [24].

$$\text{DIF} = 1 + (\frac{\varepsilon^{\cdot}}{C})^{\frac{1}{p}} \tag{9}$$

In the above equation, $\varepsilon^{\cdot}$ represents the strain rate of steel. The coefficients P and C are determined from multiple experimental results and are taken as 3.585 and 808 s^{-1}, respectively.

To simulate blast loading, the ConWep model in ABAQUS was employed, with the explosion type defined as an air blast. For validation purposes, the results obtained from the ABAQUS simulations were compared with those reported by Zhang et al. [23] using LS-DYNA. In this study, the lateral displacement at the mid-height of the modeled specimen was compared with the results from the reference study. The comparison of the two curves, as shown in Figure 6, indicates that the differences between the ABAQUS and LS-DYNA results are acceptable. Therefore, the present model can be reliably used to accurately investigate the behavior of CFST columns under blast loading.

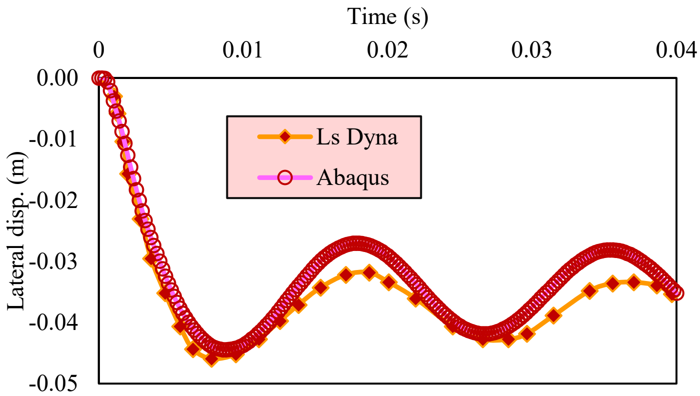

Figure 6. Comparison of the Pinned-End Model Results obtained in the Present Study with those Reported by Zhang et al. [23]

Loading

In this study, three types of loading were applied to the specimens. First, the self-weight was applied to each specimen according to Table 1. Next, the blast load was applied using the Dynamic Explicit solver in ABAQUS. For this purpose, it was assumed that the specimen was subjected to a blast from 20 kg of TNT placed at a distance of 1.5 meters. For fire loading, the standard ISO-834 fire curve was used to simulate the thermal effects. The thermal load was applied through convective heat transfer at 25 W/m² for surfaces exposed to fire and radiative heat transfer with an emissivity coefficient of 0.5.

In this study, the failure criterion was defined according to BS 476: the column is considered to have failed when the axial deformation exceeds L/20 or when the deformation rate exceeds $L^2/(9000D)$, whichever occurs first (where L is the column length and D its diameter). Figure 7 illustrates the stages of the applied loading.

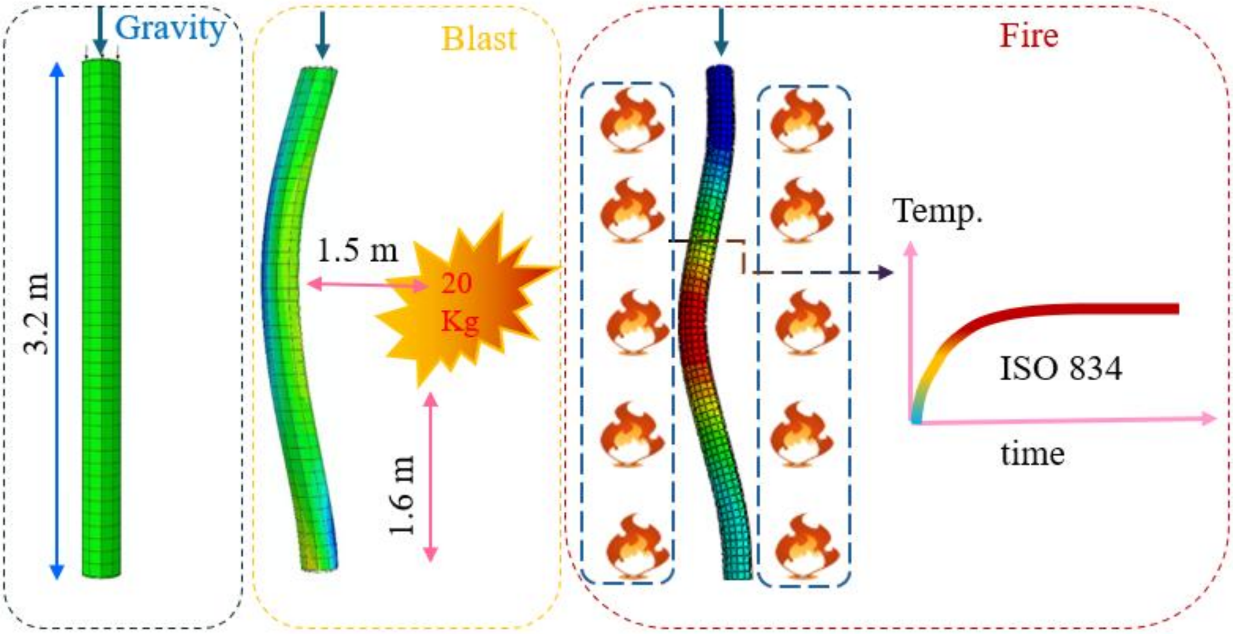

Figure 7. Loading Stages in the Post-Blast Fire Scenario

Probabilistic and Sensitivity Analysis

In this study, an effort was made to investigate the resistance of CFST columns probabilistically, taking into account inherent uncertainties. The Monte Carlo simulation method, which generates random numbers and repeatedly samples the input random variables—including loading and material properties - enables a comprehensive assessment of engineering system behavior under uncertain conditions. The advantage of this approach over deterministic methods lies in its ability to quantify the probability of failure and perform risk analysis, allowing designers and decision-makers to optimally enhance the safety and reliability of structures.

In this research, material and loading parameters were considered as sources of uncertainty, and the failure time was derived as a structural resistance function in the form of a probability distribution. The steel yield stress and elastic modulus, as well as the concrete compressive strength, were selected as random material variables. The self-weight load was also defined as an uncertainty. Additionally, the cross-sectional dimensions and thickness were considered as uncertainties in this study. The distributions, mean values, and coefficients of variation of these variables are presented in Table 3.

Table 3. Characteristics of the Random Variables [17,37,38,39]

Category	Item	Property	Mean	COV (%)	Dist. type
	Steel	fy	358 MPa	10	Lognormal
Materials	Steel	E	2e5 MPa	5	Normal
	Concrete	fc	48 MPa	10	Lognormal
Load	Gravity		820 kN	10	Normal
Geometry	Thickness		4 mm	5	Gamma
	Dimension		200 mm	5	Gamma

To investigate the influence of each random variable on the failure time of the main specimen, a sensitivity analysis was conducted using the tornado diagram approach (TDA). TDA is a widely used first-order sensitivity analysis method, commonly employed in decision analysis [40-41]. In this method, the sensitivity of the output, in this case, the expected damage behavior (EDB), to each input parameter is presented using horizontal bar charts. A set of input variables with their corresponding probability distributions is considered. Initially, the output corresponding to the mean value of each parameter is measured and treated as the baseline. Then, each parameter is individually fixed at the upper and lower bounds of its probability distribution while keeping all other parameters at their mean values. The difference in outputs between these two bounds, called the "swing," is calculated as the sensitivity of the selected parameter. Finally, input parameters are ranked based on their swing values. Detailed information on TDA sensitivity analysis can be found in references [40].

Assessment of Member Behavior under Blast and Fire Scenarios

Before performing a probabilistic assessment of the column resistance, a deterministic evaluation was carried out to investigate the behavior and strength of the specimens and the influence of varying parameters. The behavior of specimens C1 and C2 under the post-blast fire scenario was examined. Figure 8 illustrates the deformation of specimen C1 over the duration of the applied blast load. At the initial stage, due to the compressive blast load applied to the column, a significant lateral deformation is observed. As time progresses and the blast load is removed, the column continues to oscillate, with the amplitude of lateral deformation gradually decreasing in subsequent cycles. At the final stages, a residual displacement remains in the column, referred to as permanent displacement.

It was also observed that the maximum lateral displacement occurs at approximately 0.7 of the column height from the base. Therefore, in this study, in the diagrams illustrating lateral deformation of the column, the variations at this specific point are considered as representative of the overall lateral behavior.

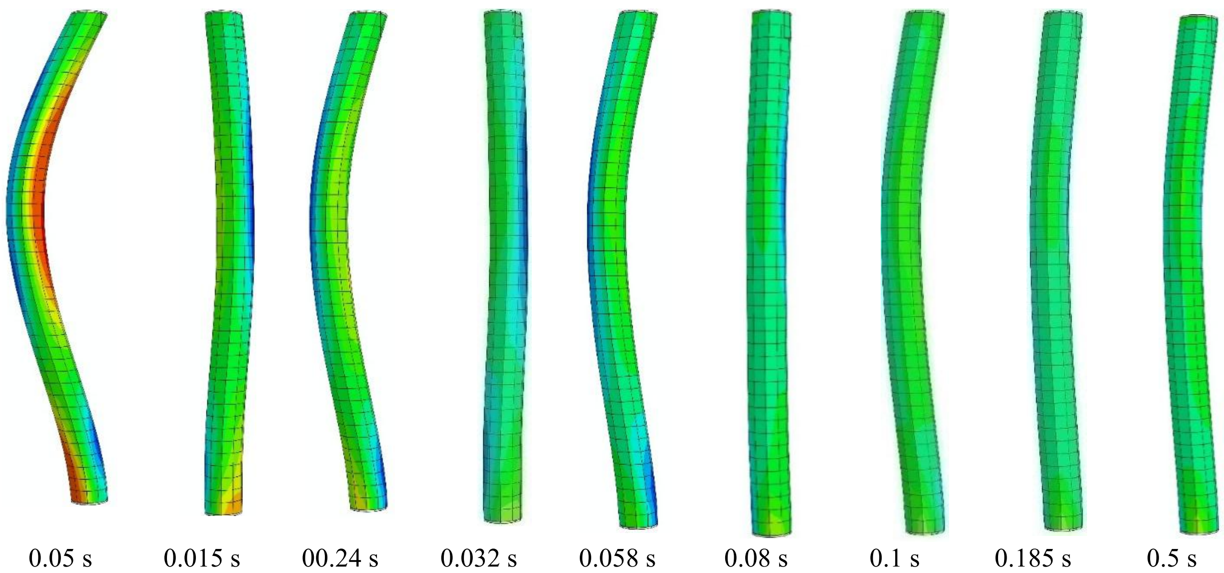

Figure 8. Lateral Displacement of Specimen C1 under Blast Loading

To assess the effect of blast loading on the fire resistance of the column, a comparison of the resistance of specimen C1 with and without prior blast loading is presented in Figure 9. As shown in Figure 9, the occurrence of a blast before fire exposure can reduce the fire resistance of CFST columns. One of the reasons is the residual displacement remaining after the blast, which may lead to premature buckling of the column. Additionally, the development of local buckling on the steel surface, particularly in columns with large cross-sections, reduces the capacity of the steel tube during global buckling.

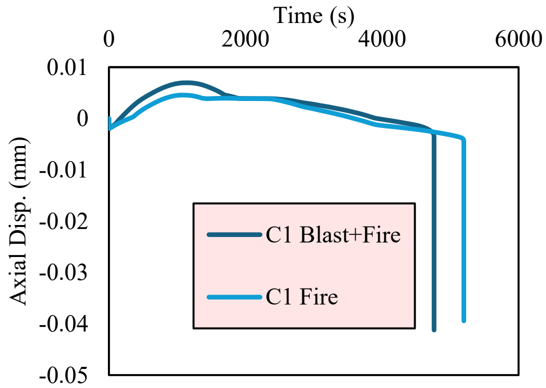

Figure 9. Axial Displacement of Specimen C1 under Fire Loading with and without Prior Blast Exposure

To compare the behavior of CFST columns with hollow steel tube columns under blast and fire loading, the specimens listed in Table 1 were considered. Specimen C2 represents the hollow steel tube column, while specimen C1 corresponds to the CFST column. To maintain a consistent design reliability factor, the applied load was set to 0.45 of the axial capacity of the column cross-section.

Figure 10 illustrates the lateral displacement history of the columns during the application of the blast load. As shown, the presence of concrete in the CFST specimen not only reduces the initial lateral displacement but also decreases subsequent displacements as well as the residual displacement. This behavior is attributed to the high lateral stiffness of the concrete core within the steel tube, which significantly increases the overall lateral stiffness of the CFST column compared to the hollow steel tube, resulting in smaller initial and residual lateral displacements.

Furthermore, compared to the hollow column, the concrete core prevents inward buckling of the steel tube, thereby avoiding local crushing and reducing the residual lateral displacement of the CFST column. In this model, since oscillations have nearly ceased after 0.5 seconds, fire loading is applied at this time. It should be noted that if the fire were applied before 0.5 seconds, the column behavior would remain essentially the same, as oscillations stop within a fraction of a second.

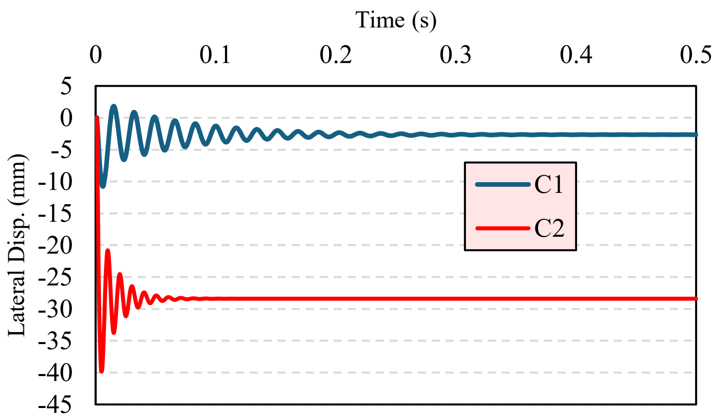

Figure 10. Lateral Displacement History of the Specimens during and after Blast Loading

Figure 11 illustrates the fire resistance of specimens C1 and C2 under post-blast fire loading. As shown, the occurrence of a blast prior to fire exposure can reduce the fire resistance of both CFST and hollow steel tube columns. It can be observed that, under the same applied load ratio of 0.45 of the axial capacity, the CFST column exhibits higher fire resistance compared to the hollow steel tube column. This improvement is attributed to the presence of concrete within the specimen, which prevents inward buckling of the steel tube and delays the global buckling of the column, thereby enhancing fire resistance.

According to Figure 11, the fire resistance of specimen C1 under fire loading alone is 5200 seconds, which decreases to 4800 seconds under the post-blast fire scenario. For specimen C2, these values are 2600 seconds and 2300 seconds, respectively. The results indicate that the blast reduces the fire resistance of specimen C1 by 8.33% and specimen C2 by 13%. This demonstrates one of the advantages of incorporating concrete into the column, as the reduction in fire resistance is less significant compared to the hollow steel tube, given the same applied load ratio.

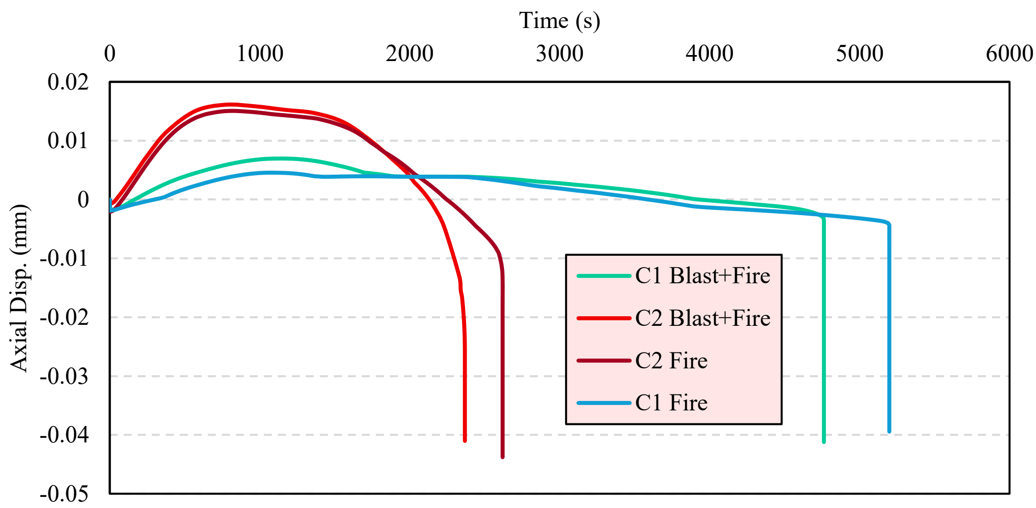

Figure 11. Axial Displacement of Specimens C1 and C2 under Fire Loading Following a Blast

To investigate the effect of column dimensions, specimens C1, C3, and C4 were analyzed. In all these specimens, the applied load ratio was kept constant at 0.45 of the axial capacity of the column cross-section. As shown in Figure 12, increasing the dimensions of the specimens reduces both the initial and residual lateral displacements caused by the blast. This behavior is attributed to the fact that the lateral stiffness of the specimen is independent of the applied compressive load. Therefore, with an increase in cross-sectional dimensions and the corresponding increase in stiffness, both the initial and residual lateral displacements are reduced.

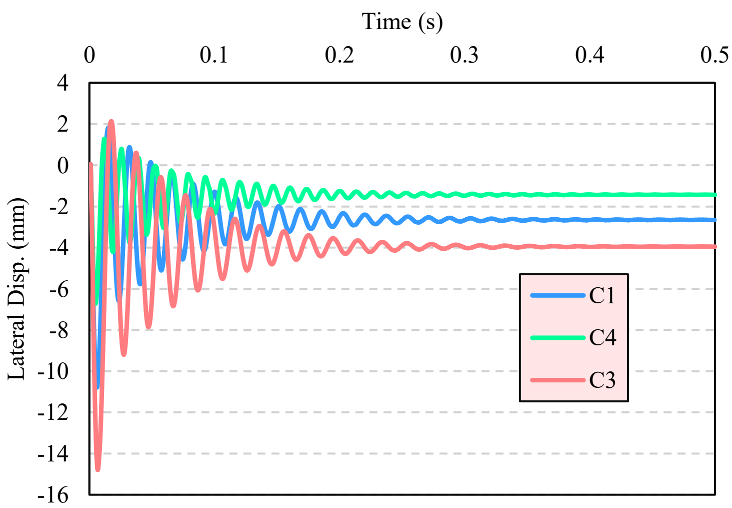

Figure 12. Lateral Displacement History of Specimens C1, C3, and C4 during and after Blast Loading

As observed in Figure 13, it is not straightforward to predict the effect of increasing the column cross-sectional dimensions. Comparing specimens C4 and C3, it is evident that specimen C1 exhibits lower fire resistance than C3. The fire resistance of specimens C1, C3, and C4 under the post-blast fire scenario was calculated as 4800, 5046, and 8893 seconds, respectively. This behavior is primarily attributed to the lower applied axial load in specimen C1. In this case, the influence of the reduced applied load outweighs the effect of increased cross-sectional area, allowing the column with a smaller compressive load to resist fire more effectively.

This phenomenon indicates that in multi-story buildings, it cannot be assumed that lower floors with larger cross-sections will necessarily exhibit higher fire resistance compared to upper floors. The presence of axial load plays a critical role, potentially offsetting the benefits of larger cross-sectional areas. However, for specimen C4, the increase in both cross-sectional area and axial load results in higher thermal resistance. This is due to the change in column behavior with increasing dimensions. Specifically, specimen C4 behaves as a short column, whereas specimens C1 and C3 behave as slender columns. In short columns, the cross-section reaches its axial capacity before global buckling occurs, leading to failure, whereas in slender columns, global buckling occurs before the cross-section attains its full axial capacity, resulting in premature failure.

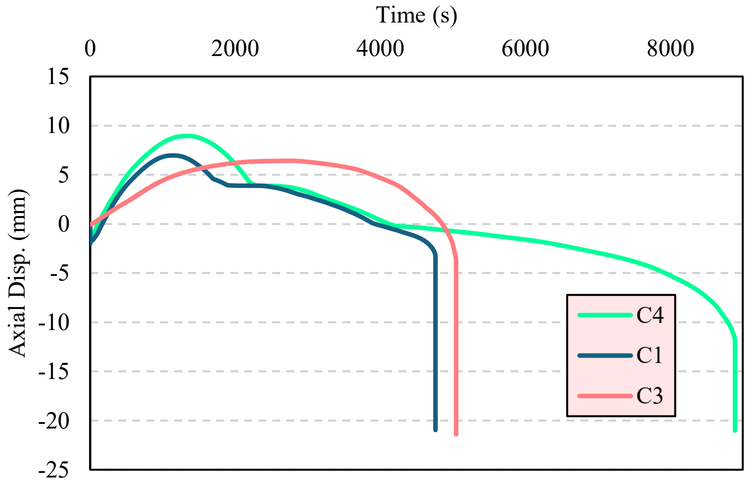

Figure 13. Axial Displacement of Specimens C1, C3, and C4 under Fire Loading

To investigate the effect of column height on the fire resistance of CFST columns under post-blast conditions, three different column heights (specimens C1, C5, and C6), detailed in Table 1, were evaluated. To maintain a consistent design reliability factor across all three columns, the slenderness ratio—dependent on support conditions, dimensions, and column height—was assumed to be the same. In other words, with identical support conditions, an increase in height was accompanied by an increase in the cross-sectional area.

Figure 14 presents the horizontal displacement curves of specimens C1, C5, and C6 under blast loading. It can be observed that, despite the increase in height, the residual displacement decreases, indicating a reduced effect of the blast on these taller specimens. This behavior is attributed to the increase in cross-sectional area with height. In other words, the increased cross-sectional dimensions enhance the lateral stiffness, compensating for the reduction in stiffness due to increased height, and thereby reducing both the initial and residual lateral displacements.

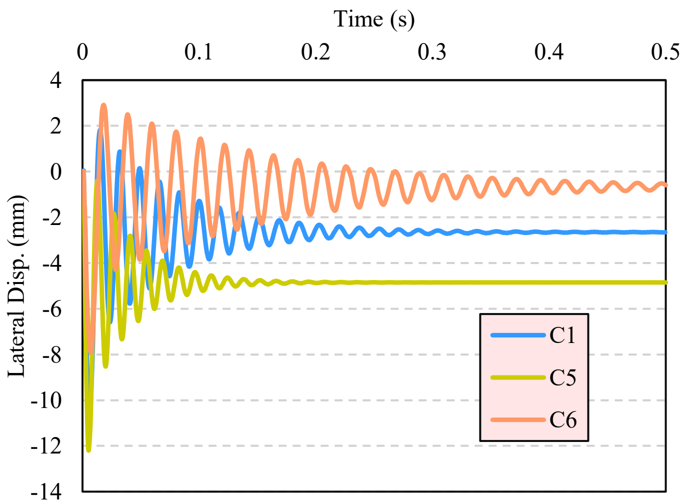

Figure 14. Lateral Displacement History of Specimens C1, C5, and C6 during and after Blast Loadin

As shown in Figure 15, increasing the column height, and consequently the cross-sectional area, enhances the fire resistance of the column. This behavior is attributed to the increased cross-sectional area, which results in a larger concrete core, delaying the global buckling of the column. The fire resistance of specimens C1, C5, and C6 under the post-blast fire scenario was found to be 4800, 4438, and 10829 seconds, respectively.

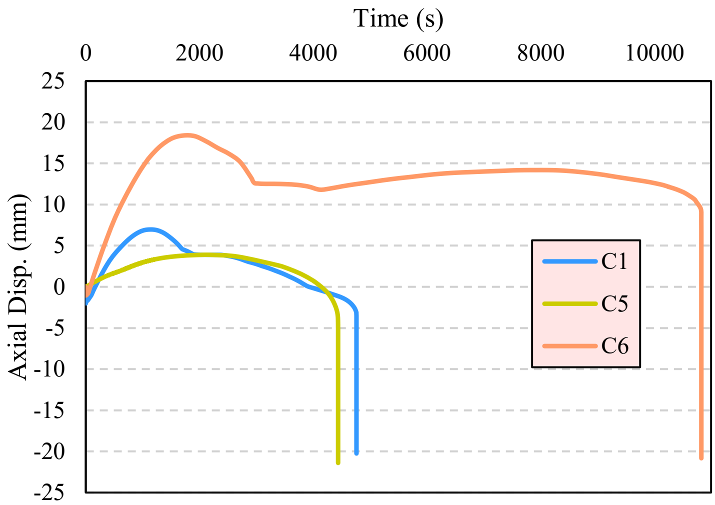

Figure 15. Axial Displacement of Specimens C1, C5, and C6 under Fire Loading

The stiffness of the column end connections is one of the key factors affecting its buckling behavior. To investigate the influence of support conditions, the top end of the column was assumed to have infinite stiffness, representing a fixed support condition (specimen C7), while in another specimen, the top end was assumed to have zero stiffness, representing a pinned support condition (specimen C1). As shown in Figure 16, which presents the lateral displacement of the columns, increasing the stiffness of the top connection reduces both the maximum lateral displacement and the residual displacement, indicating a reduced effect of the blast.

This behavior is attributed to the decrease in the column slenderness ratio due to the fixed support condition. In other words, with a lower slenderness ratio, the column behaves more like a short column, exhibiting higher buckling resistance compared to slender or tall columns.

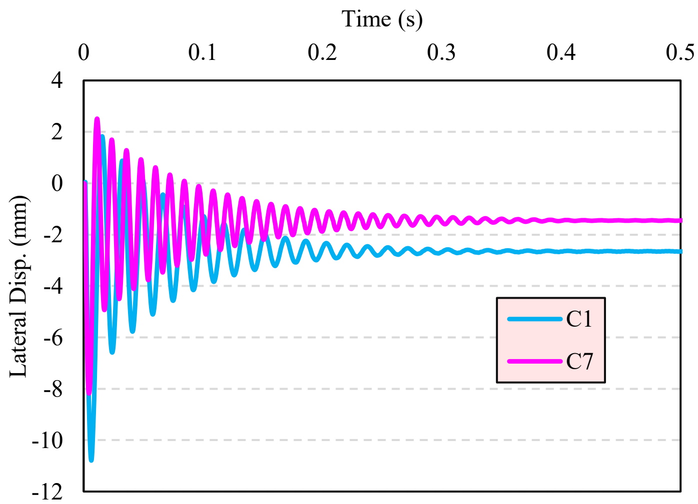

Figure 16. Lateral Displacement History of Specimens C1 and C7 during and after Blast Loading

As shown in Figure 17, fixing the top support increases the fire resistance of the column. This behavior is attributed to the increased stiffness of the top connection, which not only reduces the effect of the blast but also decreases the slenderness of the column, delaying the onset of global buckling.

Furthermore, Figure 18 illustrates the buckling mode of the column under the two different support conditions. For the fixed–fixed support, the maximum lateral displacement occurs at mid-height of the column, whereas for the fixed–pinned support, it occurs at approximately 0.7 of the column height from the base. The larger lateral displacement in the pinned–fixed case is due to the proximity of the point of maximum displacement to the pinned support and its distance from the fixed connection, which reduces the influence of the support stiffness on the column's lateral displacement compared to the fixed–fixed configuration.

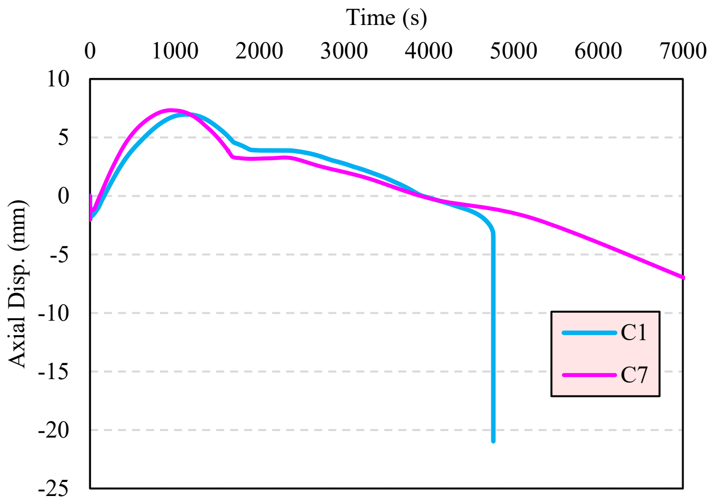

Figure 17. Axial Displacement of Specimens C1 and C7 under Fire Loadin

Figure 18. Lateral Displacement Mode of Columns with Different Support Conditions: (a) C1, (b) C7

Sensitivity Analysis

To investigate the influence of random variables on the resistance of the specimens, sensitivity analysis was conducted using the Tornado Diagram Analysis (TDA) method. The results of this analysis are presented as tornado diagrams for each specimen in Figure 19. The results indicate that as the resistance of the specimens under the post-blast fire scenario increases, the swing range (the interval between the mean minus two standard deviations and the mean plus two standard deviations) also increases.

Among the considered random variables, the elastic modulus exhibited the smallest swing in all specimens. In other words, variations in the steel elastic modulus (considering its distribution and coefficient of variation) have the least effect on the variation of structural resistance in this scenario. Based on the coefficients of variation and the distributions of the random variables, changes in column thickness and cross-sectional dimensions also have a limited impact on the resistance.

However, the most significant effects are attributed to steel yield stress, concrete compressive strength, and axial load. These three parameters notably influence the resistance of CFST columns under the post-blast fire scenario. The dominant parameter varies among specimens: in some cases, concrete strength (e.g., specimens C1, C4, and C7), in others, steel yield stress (e.g., specimen C5), and in others, axial load (e.g., specimens C2, C3, and C6) exhibits the highest sensitivity in determining structural resistance under this scenario.

Since the swing range depends on the resistance time of the members, it is more appropriate to use a sensitivity coefficient for a more precise evaluation. The sensitivity coefficient is the normalized swing relative to the mean value in each scenario. Table 4 presents the sensitivity coefficients for the different cases.

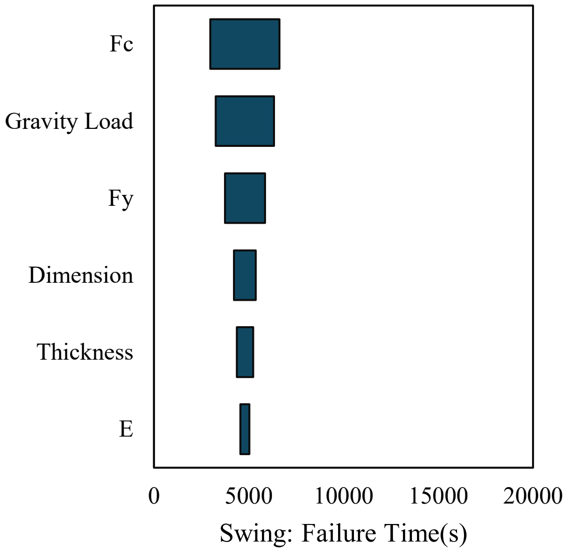

C1

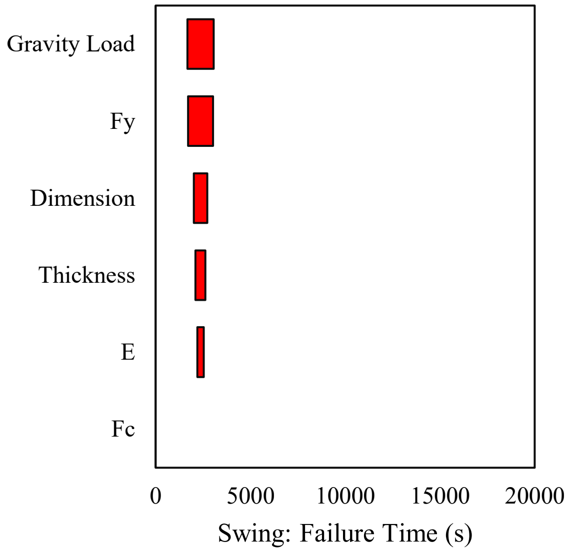

C2

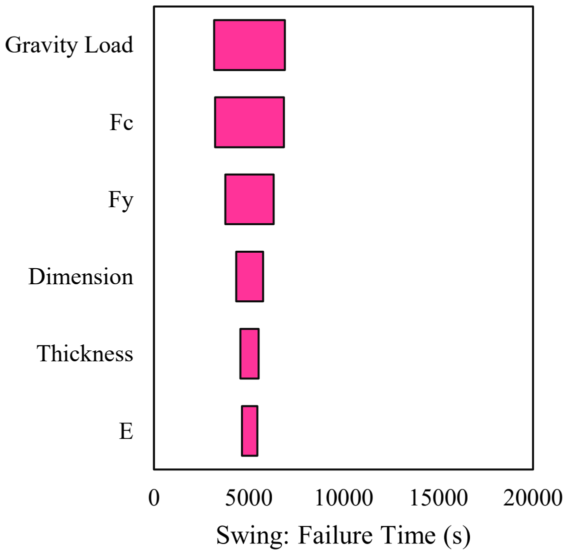

C3

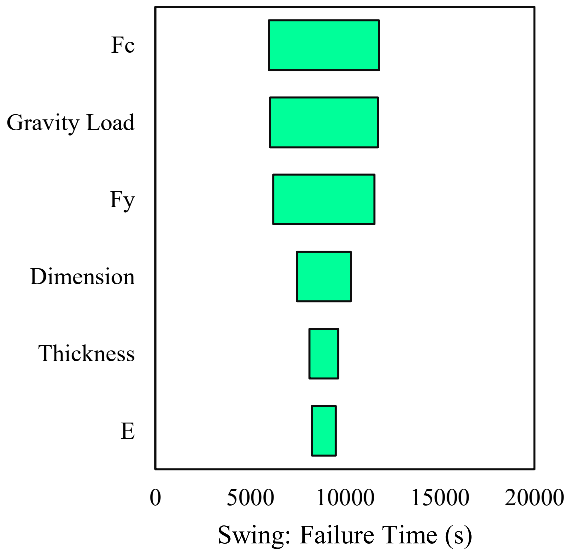

C4

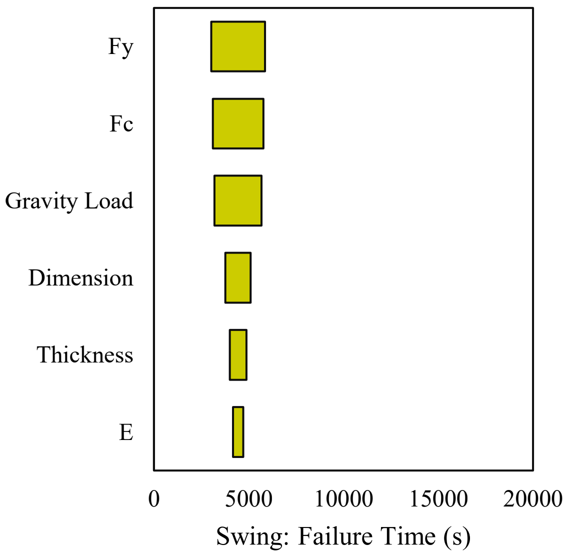

C5

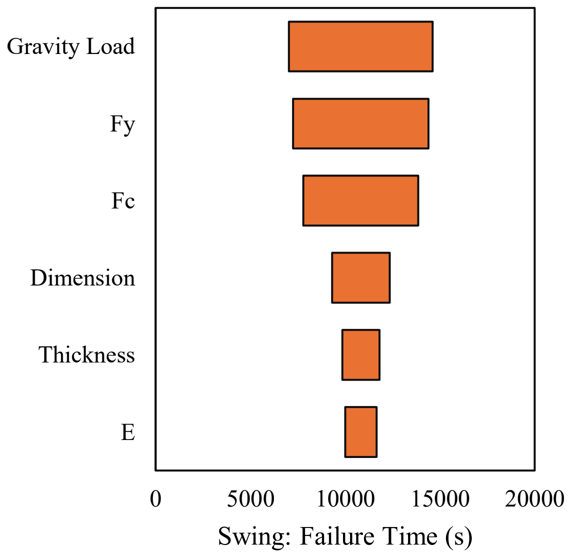

C6

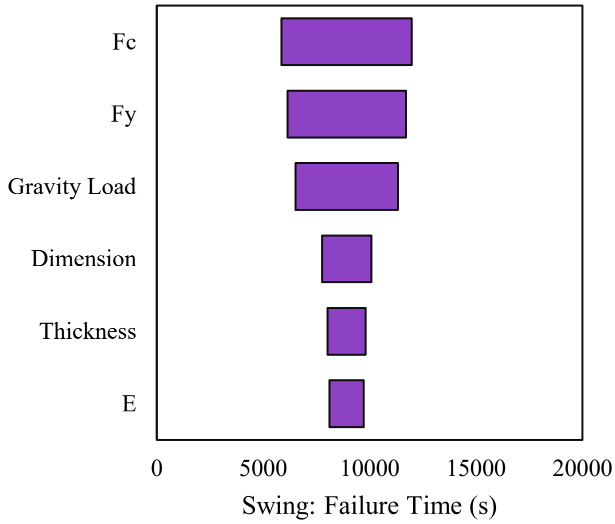

C7

Figure 19. Results of the Sensitivity Analysis using Tornado Diagram Analysis (TDA)

The results indicate that the highest sensitivity coefficient with respect to the steel yield stress (F_y) occurs for specimen C6, with a value of 0.66. The highest sensitivity with respect to concrete compressive strength (F_c) is observed in specimen C1, with a value of 0.76, which represents the maximum sensitivity among all specimens and parameters. The elastic modulus, steel thickness, and steel diameter show the highest sensitivities in specimens C7, C2, and C4, respectively, with sensitivity coefficients of 0.18, 0.22, and 0.32. The axial load exhibits the most significant effect on member resistance in specimen C3, with a sensitivity coefficient of 0.72.

Table 4. Sensitivity Coefficients of Various Parameters in Different Specimens

	C1	C2	C3	C4	C5	C6	C7
Fy	0.44	0.56	0.504	0.6	0.64	0.66	0.624
Fc	0.76	0	0.72	0.652	0.6	0.56	0.686
E	0.1	0.14	0.16	0.14	0.12	0.152	0.18
Gravity Load	0.64	0.584	0.74	0.64	0.56	0.701	0.54
Thickness	0.18	0.22	0.19	0.17	0.2	0.18	0.2
Dimension	0.24	0.3	0.28	0.32	0.3	0.28	0.26

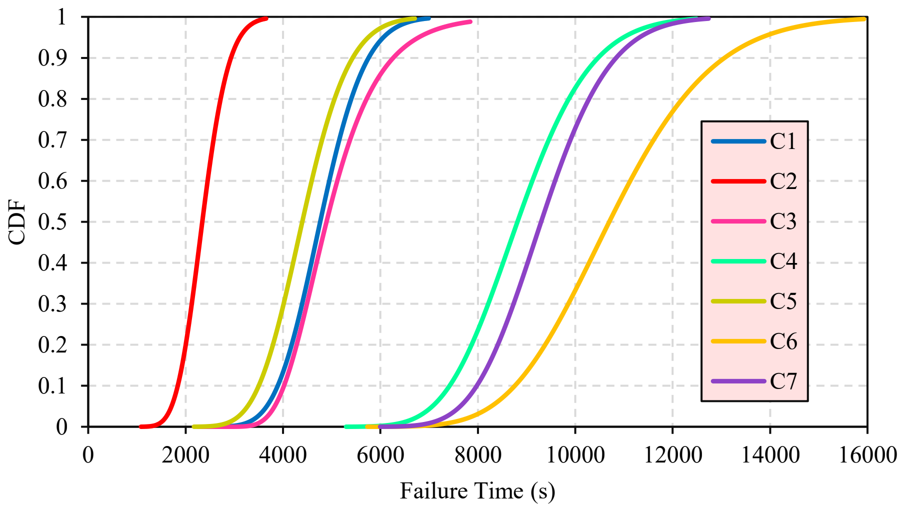

Figure 20. CDF of Failure Time for Different Specimens obtained by Monte Carlo Simulation

In Figure 20, the results of the probabilistic analysis using the Monte Carlo method are presented. This figure illustrates the cumulative distribution function (CDF) of the resistance of the specimens (failure time). As was already evident from the deterministic analyses, specimen C6 exhibits the highest resistance, while specimen C2 shows the lowest. This trend is also clearly reflected in the probabilistic results.

The CDF curves indicate the probability of a specimen failing within a time shorter than a given threshold. For instance, in specimen C4, the probability of failure occurring before 10,000 seconds is 82%. This probability equals 71% for specimen C7, 32% for specimen C6, and 100% for the remaining specimens.

The analysis results further demonstrate that at the time when specimen C2 (the hollow steel tube) has a 100% probability of failure, specimen C1 (the concrete-filled counterpart of the same section) shows a 0% probability of failure. This clearly highlights the significant improvement in fire resistance after explosion when concrete is used inside the steel sections.

CONCLUSIONS

This study presented a comprehensive numerical and probabilistic investigation into the behavior of Concrete-Filled Steel Tube (CFST) columns subjected to post-blast fire loading. A validated sequential finite element framework was developed in ABAQUS to capture the coupled effects of blast-induced damage and subsequent fire exposure. The findings highlight the critical influence of prior blast loading, which reduces fire resistance by inducing residual deformations and localized buckling that accelerate failure during heating.

The presence of concrete infill significantly enhanced structural performance compared with hollow steel columns. Concrete confinement effectively limited lateral deformation under blast loads, delayed global buckling in the fire phase, and increased the failure time by more than 100% relative to hollow sections. These results confirm that the composite interaction between the steel tube and concrete core provides a robust resistance mechanism under combined dynamic and thermal actions.

The probabilistic analysis using Monte Carlo simulation demonstrated that variability in material and geometric parameters has a measurable effect on structural reliability. Among the considered variables, steel yield strength, concrete compressive strength, and axial load were identified as the dominant parameters influencing failure time, while changes in wall thickness and diameter had lesser impact. The sensitivity coefficients indicated that concrete strength and steel yield stress govern thermal stability, whereas the axial load controls global instability.

The parametric results also revealed that increasing column cross-sectional dimensions and end-fixity improves both blast resistance and subsequent fire endurance by reducing slenderness and delaying buckling. In particular, fixed–fixed support conditions led to smaller residual lateral displacements and longer failure times compared with fixed–pinned conditions, emphasizing the role of boundary stiffness in multi-hazard performance.

Overall, this research provides a validated and reliability-based framework for evaluating CFST columns under sequential blast–fire scenarios. The study clarifies the mechanisms through which prior blast damage affects fire resistance and establishes quantitative insights into parameter sensitivity and probabilistic failure. The results contribute to advancing performance-based multi-hazard design and provide a foundation for future optimization of CFST systems in safety-critical infrastructure.

REFERENCES

1. Li, Z., Dong, T.F., Fu, F., and Qian, K., Dynamic Response of Cross Steel Reinforced Concrete-Filled Steel Tubular Columns under Impact under Fire, *Journal of Constructional Steel Research*, 200, 2023, 107643.
2. Tiwary, A.K. and Bhatia, S., Experimental Investigation on Post-Fire Response of Concrete-Filled Steel Tube Columns Subjected to Elevated Temperature, *Fire Technology*, 59(2), 2023, pp. 847–878.
3. Zhang, J., Liu, Y., Chen, Z., Cai, R., and Li, X., Seismic Behavior of High-Strength Concrete-Filled Square Steel Tube Columns Reinforced with Ultrahigh-Strength Bars, *Structures*, 34, 2021, pp. 3125–3140.
4. Van Cao, V. and Thong, T., Performance of Circular Concrete-Filled Steel Tubes after Fire Exposure: Experiments, *Structures*, 55, 2023, pp. 1331–1341.
5. Shintani, Y., Nishimura, T., Okazaki, T., Kinoshita, T., Ito, H., and Liew, J.R., Experimental Study on Fire Resistance of Unprotected Concrete-Filled Steel Tubular Columns under Multi-Loading, *Fire Safety Journal*, 120, 2021, 103174.
6. Tang, C.W., Fire Resistance of High-Strength Concrete-Filled Steel Tubular Columns under Combined Temperature and Loading, *Steel and Composite Structures*, 27(2), 2018, pp. 243–253.
7. Goto, Y., Mizuno, K., and Prosenjit, K., Nonlinear Finite-Element Analysis for Cyclic Behavior of Thin-Walled Stiffened Rectangular Steel Columns with Infilled Concrete, *Journal of Structural Engineering*, 138(5), 2012, pp. 571–584.

8. Mao, W.J., Wang, W.D., Zhou, K., and Du, E.F., Experimental Study on Steel-Reinforced Concrete-Filled Steel Tubular Columns under Fire, *Journal of Constructional Steel Research*, 185, 2021, 106867.
9. Wang, T., Yu, M., Zhang, X., Xu, L., and Huang, L., Experimental Study and Proposal of a Design Model of Ultra-High Performance Concrete Filled Steel Tube Columns Subjected to Fire, *Engineering Structures*, 280, 2023, 115697.
10. Wang, H., Wu, C., Zhang, Fang, Q., Xiang, H., Li, P., Li, Z., Zhou, Y., Zhang, Y., and Li, J., Experimental Study of Large-Sized Concrete-Filled Steel Tube Columns under Blast Load, *Construction and Building Materials*, 134, 2017, pp. 131–141.
11. Cui, Y., Song, M., Qu, Z., Sun, S., and Zhao, J., Damage Assessment of CFST Columns Subjected to Near-Field Blast Loading, *Shock and Vibration*, 2020, 2020, 8883711.
12. Chen, W., Zhou, Z., Zou, H., and Guo, Z., Predictions of Residual Carrying-Capacities for Fire and Near-Field Blast-Damaged Reactive Powder Concrete-Filled Steel Tube Columns, *International Journal of Protective Structures*, 9(4), 2018, pp. 525–553.
13. Moradi, M., Tavakoli, H., and Abdollahzadeh, G., Sensitivity Analysis of RC-Frame Failure Time under Post-Earthquake Fire Loading, *Structural Concrete*, 21(2), 2020, pp. 625–641.
14. Moradi, M., Tavakoli, H., and Abdollahzadeh, G., Probabilistic Evaluation of RC-Frame Failure Time in Post-Earthquake Fire Scenario, *Structural Concrete*, 25(5), 2024, pp. 3487–3504.
15. Moradi, M., Tavakoli, H., and Abdollahzadeh, G.R., Collapse Probability Assessment of a 4-Story RC Frame under Post-Earthquake Fire Scenario, *Civil Engineering Infrastructures Journal*, 55(1), 2022, pp. 121–137.
16. Moradi, M., Tavakoli, H.R., and Abdollahzadeh, G.R., Comparison of Steel and Reinforced Concrete Frames' Durability under Fire and Post-Earthquake Fire Scenario, *Civil Engineering Infrastructures Journal*, 54(1), 2021, pp. 145–168.
17. Moradi, M., Tavakoli, H., and Abdollahzadeh, G., Probabilistic Assessment of Failure Time in Steel Frame Subjected to Fire Load under Progressive Collapse Scenario, *Engineering Failure Analysis*, 102, 2019, pp. 136–147.
18. Craveiro, H.D., Rodrigues, J.P.C., and Vila Real, P.M.M., Structural Fire Performance of Concrete-Filled Built-Up Cold-Formed Steel Columns, *Materials*, 15(6), 2022, 2159.
19. Cai, J., Yu, Q., Zhao, X., and Lu, G., Axial Compressive Behaviours of Engineered Cementitious Composites-Encased Concrete-Filled Steel Tube Columns after Fire Exposure, *Engineering Structures*, 252, 2022, 113618.
20. Tkalenko, V., Lutsenko, I., and Golyaka, R., Analytical Model for Steel Fibre-Reinforced Concrete-Filled Tubular Columns Exposed to Fire, *European Journal of Engineering and Technology Research*, 8(4), 2023, pp. 117–123.
21. Boursas, F., Chergui, A., and Yahiaoui, S., The Influence of Slenderness in Steel and Composite Columns under Fire Conditions, Engineering, *Technology & Applied Science Research*, 13(3), 2023, pp. 11053–11057.
22. Le, V.L., Lee, C.H., Alemayehu, R.W., and Park, M.J., Finite Element Modeling of the Behaviors of Concrete-Filled Steel Tube (CFT) Columns at Elevated Temperatures, *Buildings*, 15(1), 2024, 11.
23. Zhang, J., Jiang, S., Chen, B., Li, C., and Qin, H., Numerical Study of Damage Modes and Damage Assessment of CFST Columns under Blast Loading, *Shock and Vibration*, 2016, 2016, 3972791.
24. Wang, K. and Young, B., Fire Resistance of Concrete-Filled High Strength Steel Tubular Columns, *Thin-Walled Structures*, 71, 2013, pp. 46–56.
25. Lie, T.T. and Chabot, M., *Experimental Studies on the Fire Resistance of Hollow Steel Columns Filled with Plain Concrete*, National Research Council Canada, Institute for Research in Construction, 1992.
26. Eurocode 3: *Design of Steel Structures - Part 1-2: Structural Fire Design*, European Committee for Standardization, Brussels.
27. Eurocode 2: *Design of Concrete Structures - Part 1-2: Structural Fire Design*, CEN, Brussels.
28. *Eurocode 4: Design of Composite Steel and Concrete Structures - Part 1-2: Structural Fire Design*, British Standards Institution, London.
29. Hong, S. and Varma, A.H., Analytical Modeling of the Standard Fire Behavior of Loaded CFT Columns, *Journal of Constructional Steel Research*, 65(1), 2009, pp. 54–69.
30. Lie, T.T. and Irwin, R.J., Fire Resistance of Rectangular Steel Columns Filled with Bar-Reinforced Concrete, *Journal of Structural Engineering*, 121(5), 1995, pp. 797–805.
31. Lee, J. and Fenves, G.L., Plastic-Damage Model for Cyclic Loading of Concrete Structures, *Journal of Engineering Mechanics*, 124(8), 1998, pp. 892–900.
32. Eurocode 2: *General Rules and Rules for Buildings*, British Standards Institution, London.
33. Anderberg, Y. and Thelandersson, S., *Stress and Deformation Characteristics of Concrete at High Temperatures*, 1976.
34. Ellobody, E., Young, B., and Lam, D., Behaviour of Normal and High Strength Concrete-Filled Compact Steel Tube Circular Stub Columns, *Journal of Constructional Steel Research*, 62(7), 2006, pp. 706–715.

35. Ghojel, J., Experimental and Analytical Technique for Estimating Interface Thermal Conductance in Composite Structural Elements under Simulated Fire Conditions, *Experimental Thermal and Fluid Science*, 28(4), 2004, pp. 347–354.
36. Song, T.Y., Han, L.H., and Yu, H.X., Concrete Filled Steel Tube Stub Columns under Combined Temperature and Loading, *Journal of Constructional Steel Research*, 66(3), 2010, pp. 369–384.
37. Guo, Q. and Jeffers, A.E., Finite-Element Reliability Analysis of Structures Subjected to Fire, *Journal of Structural Engineering*, 141(4), 2015, 04014129.
38. Kim, J., Park, J.H., and Lee, T.H., Sensitivity Analysis of Steel Buildings Subjected to Column Loss, *Engineering Structures*, 33(2), 2011, pp. 421–432.
39. Wardaya, D.A.S., Sugiharto, H., and Pudjisuryadi, P., Compressive Strength of Post Fire Exposed Concrete Column Wrapped with Fiber Reinforced Polymer, *Civil Engineering Dimension*, 19(2), 2017, pp. 105–110.
40. Eldin, M.N. and Kim, J., Sensitivity Analysis on Seismic Life-Cycle Cost of a Fixed-Steel Offshore Platform Structure, *Ocean Engineering*, 121, 2016, pp. 323–340.
41. Moradi, M. and Rezaei, S., The Effect of Considering Soil-Structure Interaction on the Seismic Performance, Sensitivity, and Fragility of High-Rise Structures under Near-Fault Records, *Structures,* 87, 2026, pp. 111548.